Influence of Dynamic and Thermal Forcing on the Meridional Transport of Taklimakan Desert Dust in Spring and Summer

TIANGANG YUAN, SIYU CHEN, JIANPING HUANG, AND DONGYOU WU

Key Laboratory for Semi-Arid Climate Change of the Ministry of Education, Lanzhou University, Lanzhou, China

HUI LU

Institute of Desert Meteorology, China Meteorological Administration, Urumqi, China

GUOLONG ZHANG, XIAOJUN MA, ZIQI CHEN, AND YUAN LUO

Key Laboratory for Semi-Arid Climate Change of the Ministry of Education, Lanzhou University, Lanzhou, China

XIAOHUI MA

Karamay Meteorological Bureau of Xinjiang Province, Karamay, China

(Manuscript received 3 June 2018, in final form 15 November 2018)

ABSTRACT

The Weather Research and Forecasting Model coupled with chemistry (WRF-Chem) associated with in situ measurements and satellite retrievals was used to investigate the meridional transport of Taklimakan Desert (TD) dust, especially in summer. Both satellite observations and simulations reveal that TD dust particles accumulate over the Tibetan Plateau (TP) and the Tianshan Mountains in summer, resulting in higher dust concentration up to 85 $\mu g\,m^{-3}$ here. The proportions of meridional transport of TD dust in summer increase up to 30% of the total output dust over the TD. Further, the impacts of thermal and dynamic forcing on the meridional transport of TD dust to the TP and Tianshan Mountains are investigated based on composite analysis and numerical modeling. It is found that the weakness of the westerly jet over East Asia significantly decreases the eastward transport of TD dust. More TD dust particles lifted to higher altitude reach up to 8 km induced by the enhanced sensible heating in summer. Under the influence of the northerly airflow over the TD regions, the TD dust particles are strengthened southward and transported to the northern slope of the TP through topographic forcing. Moreover, the cyclonic circulation raises dust particles to higher altitude over the TP. It can further intensify the TP heat source by direct radiative forcing of dust aerosols, which may have a positive feedback to the southward transport of TD dust. This research provides confidence for the investigation of the role of TP dust with regard to the radiation balance and hydrological cycle over East Asia.

1. Introduction

Dust aerosols, which are major component of tropospheric aerosols, are emitted into the atmosphere from wind erosion in arid and semiarid areas (Bi et al. 2011; Huang et al. 2006a, 2007, 2014; Kang et al. 2017). These aerosols can directly affect Earth's radiative budget through scattering and absorbing shortwave and longwave radiation (i.e., direct effects) (Ramanathan et al. 2001; Huang et al. 2009; Zhao et al. 2010; Chen et al. 2014a, 2017a,b,c), modifying the albedos and lifetimes of clouds by changing ice cores and cloud condensation nuclei (i.e., indirect effects) (Huang et al. 2006a,b, 2014), and even evaporating cloud droplets when aerosols appear within or above clouds (i.e., semi-direct effects) (Huang et al. 2006c), all of which have significant effects on climate change at the regional and even global scales (Huang et al. 2010, 2011, 2014; Guo and Yin 2015; Chen et al. 2014b, 2017b; Zhao et al. 2018; Gu et al. 2016). Numerous studies have reported that the long-range

Denotes content that is immediately available upon publication as open access.

Corresponding author: Siyu Chen, chensiyu@lzu.edu.cn

DOI: 10.1175/JCLI-D-18-0361.1

transport of dust can provide mineral elements (such as Fe and Al) to the oceans, thereby enhancing the oceanic biological pump (Duce et al. 1980; Wang et al. 2012; J. Li et al. 2012), and such aerosols can also clean local gaseous pollutants by reducing the SO_2/PM_{10}, NO_2/PM_{10}, and $PM_{2.5}/PM_{10}$ ratios (Guo et al. 2004). However, dust aerosols also have adverse effects on the air quality and human health by long-range transport (Kameda et al. 2016; Prospero 1999; Fu et al. 2010).

The Taklimakan Desert (TD), which is one of the major sources of dust storms over East Asia (Zhang et al. 1997; Wang et al. 2008; Huang et al. 2017), is located in the Tarim basin in northwestern China and is surrounded by the Tibetan Plateau (TP), Pamir Plateau, Tianshan Mountains, and Kunlun Mountains (average elevation $>$ 5000 m). Based on surface observations in China, the dust emission intensity over the TD is the strongest, followed by the Gobi Desert (GD), especially in the spring and summer (Yuan et al. 2016). Previous studies always focused on the long-range transport of TD dust in the spring and indicated that dust particles originating from the TD primarily sweep across eastern China and are eventually transported to the Pacific Ocean (Sun et al. 2001; Huang et al. 2008a; Zhao et al. 2006) and even to North America and the Atlantic by westerly winds (Yumimoto et al. 2009). Chen et al. (2017a) further pointed out that the dust emission abilities of the TD are the largest among all of the regions in East Asia, as the TD accounts for 42% of all dust emissions over East Asia. However, compared with the GD, TD dust particles below 5 km cannot be easily transported eastward due to the special terrain and the prevailing easterly winds at low atmospheric altitudes (Sun et al. 2001; Ge et al. 2014).

To investigate new transport paths of TD dust over East Asia, Huang et al. (2007) examined *Cloud–Aerosol Lidar and Infrared Pathfinder Satellite Observations* (*CALIPSO*) retrievals and first found that TD dust can be entrained to 9 km and then be transported toward the south to the northern slopes of the TP in the summer. Liu et al. (2008) further found that the TD is the primary dust contributor to the TP. Moreover, the aerosol optical depth (AOD) over the TP has a closer correlation with that over the TD in the summer than that in the spring (Xia et al. 2008). Simulations further showed that the transport of TD dust to the TP in the summer of 2006 was favored by the thermal effect of the TP and the weakness of westerly winds (Chen et al. 2013), which showed a high correlation with the cold front–based transport of dust sources to the north slopes of the TP (Jia et al. 2015). Because of the high elevation, the dust particles over the TP can be easily transported to remote areas, such as the Pacific Ocean, which can enhance the biological pump, further influencing the global warming (Han et al. 2004; Fang et al. 2004).

Previous studies mainly focus on the zonal transport and little attention has been paid to the meridional transport of TD dust. How do the characteristics of the transport of TD dust vary in different directions near the Tarim Basin, especially the differences between spring and summer? What are the mechanisms for the meridional transport of TD dust? The aim of this paper is to solve these questions based on the Weather Research and Forecasting Model coupled to Chemistry (WRF-Chem) in combination with various satellite retrievals and surface observations. The remainder of this paper is organized as follows. Section 2 describes the methodology and observational data used in this study. Section 3 presents the results. The conclusions and discussion are illustrated in section 4. This research may quantitatively extend our knowledge regarding the meridional transport of TD dust and its differences between the spring and summer.

2. Data and methodology

a. Model descriptions

The WRF-Chem model, which includes photolysis schemes, gas-phase chemical mechanisms, and aerosol mechanisms, considers a variety of coupled physical and chemical processes such as aerosol emission and transport (i.e., advection, diffusion, and convection), dry/wet deposition, chemical processes, aerosol interactions, and radiation forcing (Grell et al. 2005). The prominent advantage of the WRF-Chem model is that online coupling of meteorology and chemistry, which can more accurately represent the evolution of trace gases and aerosols, can indicate the feedback between aerosols and meteorological fields more effectively than other numerical models (Fast et al. 2006). The detailed parameterization schemes used in WRF-Chem are illustrated in Table 1.

The Regional Acid Deposition Model version 2 (RADM2) photochemical chemical mechanisms and Model Aerosol Dynamics Model for Europe (MADE) with the Secondary Organic Aerosol Model (SORGAM) (jointly MADE/SORGAM) were integrated into the WRF-Chem model. The MADE/SORGAM, with aerosol species including black carbon (BC), organic matters, dust, sea salt, sulfate, nitrate, and ammonium, uses the Aitken, accumulation, and coarse modes to describe the aerosol size distribution (Grell et al. 2005). The anthropogenic emissions of BC, organic carbon (OC), volatile organic compounds (VOCs), NO_x, SO_2, CO, $PM_{2.5}$, and PM_{10} derived from the Reanalysis of the Tropospheric (RETRO) chemical composition inventories are considered

TABLE 1. Model configuration.

Physicochemical process	Parameter scheme
Microphysics	Morrison two-moment (Morrison et al. 2005)
Cumulus convection	Kain–Fritsch (Kain and Fritsch 1990; Kain 2004)
Planetary boundary	Yonsei University (Hong et al. 2006)
Land surface	Noah land surface model (Chen et al. 1996; Chen and Dudhia 2001)
Longwave and shortwave radiation	RRTMG (Rapid Radiative Transfer Model for GCMs) (Mlawer et al. 1997; Iacono et al. 2000)
Gas-phase chemistry	Regional acid deposition model 2 photochemical reaction mechanism (RADM2) (Grell et al. 2005)
Aerosol chemistry	Model Aerosol Dynamics Model for Europe (MADE), with the secondary organic aerosol model (SORGAM) (Grell et al. 2005)

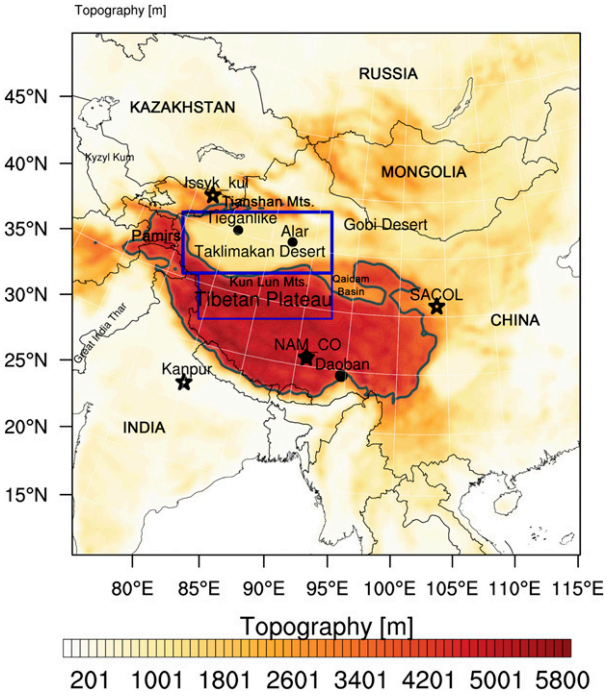

FIG. 1. Modeling domain and the topography distribution. The blue rectangles represent the Taklimakan Desert and Tibetan Plateau, respectively; the stars represent the Aerosol Robotic Network (AERONET) stations, and the black solid circles are the surface weather stations at Tieganlike and Alar in the TD and Nam Co and Daoban in the TP; the dark slate gray line is terrain height of TP above 3500 m, the same is true for all following figures.

in the WRF-Chem model. Monthly biomass burning emissions are obtained from the Global Fire Emissions Database, Version 3 (GFEDv3) (van der Werf et al. 2010). The Goddard Chemistry Aerosol Radiation and Transport (GOCART) dust emission scheme (Ginoux et al. 2001) has the ability to describe the spatial and temporal variations in dust emissions, transport, and deposition over North Africa, North America and East Asia (Chen et al. 2013, 2014b, 2017a; Zhao et al. 2010, 2011). Aerosol chemistry is initialed by the default profiles in WRF-Chem. The modeling domain covers the area of 10°–59°N, 51°–125°E with a resolution of 36 km × 36 km, and it spans 35 vertical profiles up to 100 hPa (Fig. 1). The National Centers for Environmental Prediction Final Operational Global analysis (NCEP FNL) datasets with a horizontal resolution of 1° × 1° at 6-h temporal intervals were used to supported the initial meteorological fields and lateral boundary conditions. The simulated time ranged from 1 June 2006 to 31 December 2011. Only the results output from the WRF-Chem model in the spring (March–May) and summer (June–August) during 2007–11 were used in this paper. Detailed information of the model design can be obtained from Chen et al. (2017a).

b. *Observations*

1) MODIS

The Moderate Resolution Imaging Spectroradiometer (MODIS) instrument on board the *Terra* and *Aqua* satellites views the entire Earth surface every 1 to 2 days while acquiring data in 36 spectral bands ranging from 0.4 to 15 μm representing three spatial resolutions: 250 m (2 channels), 500 m (5 channels), and 1 km (29 channels). The MODIS aerosol products monitor the ambient aerosol loading and some other aerosol properties over cloud-free and snow/ice-free land and ocean surfaces (Kaufman et al. 2005; X. Li et al. 2012). Furthermore, the Deep Blue (DB) algorithm is used to determine the properties of aerosols over land, including bright surfaces (Hsu et al. 2006, 2013). Therefore, the AODs based on the DB algorithm from MODIS/*Aqua* level 3 collection 6 products at 550 nm with a resolution of 1° × 1° resolution were used to verify the model results.

2) MISR

The Multiangle Imaging Spectroradiometer (MISR) instrument successfully launched on board *Terra* on 18 December 1999, provides radiometrically and geometrically calibrated images in spectral bands at each angle (Diner et al. 2005; Martonchik et al. 2002; Xu et al. 2013). MISR data are effective at distinguishing the reflectance contributions from the top of the atmosphere from those of the surface and atmosphere and at retrieving aeroso properties,

even over highly reflective surfaces such as deserts by virtue of nine widely spaced angles (Martonchik et al. 2002, 2004). AOD data from the MISR level 3 version 31 product with a resolution of 0.5° × 0.5° were also used.

3) CALIPSO

CALIPSO, launched in April 2006, carries the Cloud–Aerosol Lidar with Orthogonal Polarization (CALIOP) instrument, which can detect the vertical profiles of aerosols extinction coefficient at 532 and 1064 nm (Vaughan et al. 2004; Winker et al. 2003). It can also distinguish aerosols species including dust, polluted dust, clean marine, clean continental, polluted continental, and smoke. The *CALIPSO* level 2 aerosol profile product version 4.10 from 2007 to 2016 is used in this study. Huang et al. (2015) suggested that the cloud aerosol discrimination (CAD) score, which reveals the confidence of the aerosol or cloud, larger than 70 is reasonable. Besides, extinction quality control (QC) flags are also provided for the solutions if the retrieval is constrained (QC = 1) or the lidar ratio unchanged during the extinction retrieval (QC = 0) (Chen et al. 2013). The dust AOD can be calculated by integrating the dust extinction coefficient (DEC) over the height of the dust layer.

4) AERONET

The Aerosol Robotic Network (AERONET) is a global ground-based aerosol monitoring network established by the U.S. National Aeronautics and Space Administration (NASA) (Holben et al. 1998). The radiances observed from sun photometers are further used to retrieve aerosol properties based on the algorithms developed by Dubovik and King (2000). The network imposes a standardization of the instruments, calibration, processing, and distribution. AOD products are available at three levels based on the data quality: unscreened data (Level 1.0), cloud-screened data (Level 1.5), and quality-assured and cloud-screened data (Level 2.0). In this work, the Level 2.0 AOD products at the Issyk-Kul, Kanpur, Nam Co, and Semi-Arid Climate Observatory and Laboratory (SACOL) sites (Table 2) were used to evaluate the simulated AODs.

5) METEOROLOGY

The daily temperature at 2 m and surface precipitation observations during 2007–11 in surface weather stations over the TD and TP are derived from the China Meteorological Administration (http://data.cma.cn/). Four stations (Daoban, Nam Co, Alar, and Tieganlike) are selected for evaluating model performance in simulating the daily variation of temperature over the TD and TP (Table 2). The National Centers for Environmental Prediction (NCEP)–National Center for Atmospheric Research (NCAR) reanalysis 1 data of wind, air temperature, geopotential height, and surface sensible heat flux with horizontal resolution of 2.5° × 2.5° from 2007 to 2016 are also used for composite analysis (Kalnay et al. 1996).

TABLE 2. The locations of the AERONET sites and weather stations.

Station	Position	Altitude (m)
Nam Co	30.77°N, 90.96°E	4704
Issyk-Kul	42.62°N, 76.98°E	1650
Kanpur	26.51°N, 80.23°E	123
SACOL	35.95°N, 104.14°E	1966
Daoban	29.58°N, 94.6°E	4390
Tieganlike	40.38°N, 87.42°E	846
Alar	40.33°N, 81.16°E	1012

3. Results

a. Model evaluation

To evaluate the performance of the WRF-Chem model in simulating the spatial and temporal distributions of the aerosol and meteorological conditions, the satellite retrievals, in situ observations, and reanalysis data are compared with the simulations in this study. Comparisons of the daily temperature at 2 m over the TP and the TD between the observations and the corresponding WRF-Chem simulations are shown in Fig. 2. Overall, the simulations effectively capture the daily variations in the observed temperature at 2 m. The simulated temperatures are 1.5°–2.2°C higher than the observations at Nam Co, Tieganlike, and Alar and 2.3°C lower at Daoban. The correlation coefficients between the simulations and observations at Nam Co, Daoban, Tieganlike, and Alar are 0.96, 0.96, 0.98, and 0.97 (Table 3), respectively, with a high confidence of 99%. Almost 80% and 97% of the simulated temperatures at 2 m are within a factor of 1.5 of the surface observations over the TP and the TD, respectively.

The daily average temperature at 2 m and surface precipitation over the TD and TP are also shown in Fig. 3. The temperature is higher over the TD and Qaidam basin (36°–39°N, 90°–98°E) compared with that over the TP. It increases from 14° to 30°C in summer over the TD. Over the Qaidam basin the temperature in summer is about 12°C higher than that in spring. It is intensified significantly by the sensible heating (Zhou et al. 2009) from spring to summer when the temperature increases from −6° to 18°C over the TP. Overall, the spatial distribution of temperature at 2 m over the TD and TP from WRF-Chem is consistent with the surface observations well, especially over the deserts and northern TP. This advantage

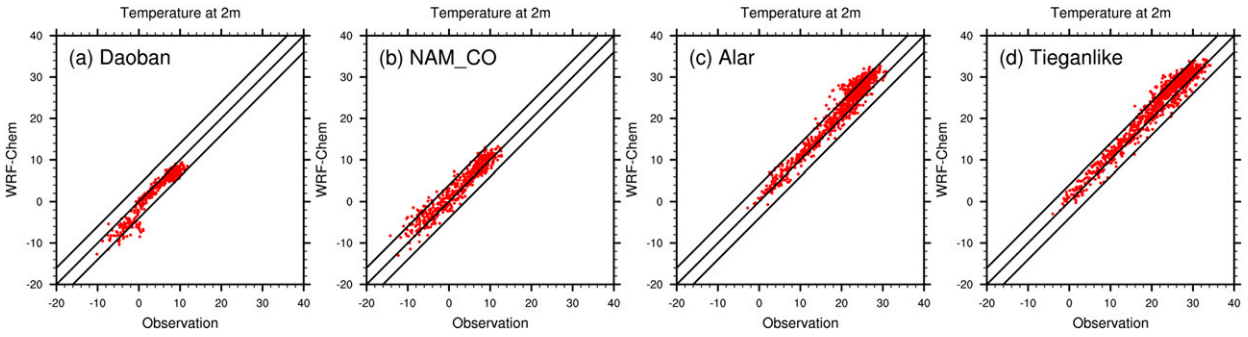

FIG. 2. The daily average temperatures (°C) at 2 m from in situ observations at (a) Daoban and (b) Nam Co over the TP, and (c) Alar and (d) Tieganlike over the TD vs the corresponding WRF-Chem simulation results during the period of 2007–11 (hereafter simulation periods). The locations of the in situ sites are shown as black solid circles in Fig. 1. The two side lines are the boundaries of deviations with −4° and 4°C, respectively.

of WRF-Chem was also demonstrated in Chen et al. (2018). The daily precipitation changes slightly in both seasons with the value less than 0.5 mm day^{-1} over the TD and Qaidam Basin. And it is even lower than 0.1 mm day^{-1} over the central deserts in spring. Both the Tianshan Mountains and the southern TP are much wet where the precipitation is up to 2 and 6 mm day^{-1} in spring and summer, respectively. The WRF-Chem model underestimates the temperature and precipitation about 8°C and 2–4 mm day^{-1} at the TP, respectively, due to the difficulty of parameterization in complex terrain. But the model still reasonably captured the spatial pattern of precipitation and temperature over the TD and TP with acceptable uncertainties.

Further, the spatial distributions of the AOD at 550 nm from MISR and MODIS retrievals and the corresponding WRF-Chem results are shown in Fig. 4. Both retrievals show that high AODs occur mainly over the TD, eastern China, the Sichuan Basin, and northern India in spring and summer. The AOD from MODIS can be up to 0.7 over the whole TD in spring while it shrinks and mainly covers the south of TD in summer. As for eastern China and northern India, which are mainly affected by anthropogenic aerosols, the AOD increases from 0.6 to more than 0.7 in summer, whereas in the Sichuan Basin the high AOD area in spring is larger than that in summer mainly owing to anthropogenic aerosols from Chengdu (Liu et al. 2016). The spatial distribution of WRF-Chem AOD is consistent with the MODIS AOD but overestimates compared with MISR AOD, especially at high AOD centers. This discrepancy is also found in Gao et al. (2016), who thought it was mainly from the uncertainties of satellites. Previous studies revealed that MISR generally underestimated the AOD compared with the AERONET AOD in China (Kahn et al. 2005; Cheng et al. 2012). X. Li et al. (2012) and Hsu et al. (2013) showed that the MODIS DB AOD had better performance over deserts regions. Moreover, the model slightly overestimates the AOD over eastern China in spring, which can be attributed the uncertainties of emission inventory. Over the north slope of the TP, Xia et al. (2008) showed the MISR performance to be better that that of MODIS and the AOD over the TP was related to the TD dust in summer. The WRF-Chem AOD in summer also extends southward to TP and it can be up to 0.5, which is consistent with the MISR AOD.

Figure 5 presents DEC at 532 nm along 84°E in summer and the seasonal differences from *CALIPSO* and the WRF-Chem results, respectively. Dust from the TD can be lifted to 7 km in summer and extends southward to TP where the DEC is 0.07 km^{-1} (Fig. 5a). Moreover, higher DEC appears at 3–8 km over the TD and TP compared with that in spring, indicating that it is easier for the dust to be lifted to high altitude and transported to northern TP in summer when the westerly jet weakens (Fig. 5b). The negative difference of DEC below 3 km at the TD

TABLE 3. Statistical value of 2-m temperature (°C) in surface weather stations.

	Observation		WRF-Chem		Correlation coefficient	
Station	Mean	Std dev	Mean	Std dev	Correlations	Significance
Daoban	4.4	4.8	2.1	5.4	0.96	0.000
Nam Co	2.5	6.1	4.4	5.8	0.96	0.000
Alar	19.5	7.1	21.7	8.0	0.97	0.000
Tieganlike	20.7	8.4	22.2	8.8	0.98	0.000

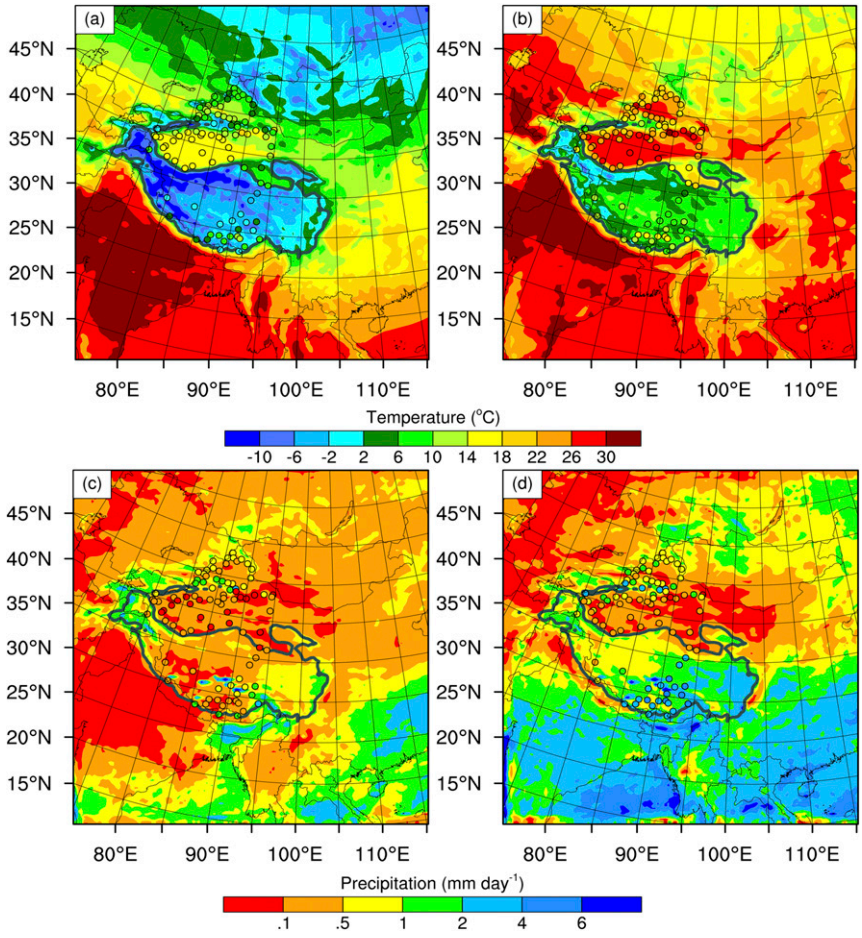

FIG. 3. Spatial distribution of average (a),(b) temperature (°C) at 2 m and (c),(d) surface precipitation (mm day^{-1}) from surface observations (dots) and the WRF-Chem model over the TD and TP in (left) spring and (right) summer during the simulation periods (focus on the TD and TP).

can be attributed to the strong dust emission in spring. Moreover, the differences are up to 0.03 km^{-1}, which is also demonstrated by WRF-Chem model. The lower DEC over northern TP from CALIPSO compared with that in the WRF-Chem model in summer may owe to excessive elimination of cloud impact. Generally, the WRF-Chem model captures the horizontal and vertical structure of the dust.

Comparisons of the monthly variation of AOD at 550 nm from the Issyk-Kul, Nam Co, Kanpur, and SACOL AERONET sites and the MODIS and MISR retrievals during 2007–11 are further shown in Fig. 6. Overall, the simulated AODs are more consistent with the surface observations with correlation coefficients exceeding 0.6 at Kanpur and SACOL than with the MODIS and MISR retrievals (Table 4). The Kanpur site is located in northern India, where anthropogenic aerosols predominate (Lu et al. 2011), and the SACOL site is located in the downwind region of the TD, where the dust events are dominant (Huang et al. 2008b). Thus, the AODs at the two AERONET sites are the highest among the four sites with average values of 0.65 and 0.46, respectively (Table 5). The Issyk-Kul site is located to the west of the Tianshan Mountains, where the dust emission is lower and the AODs range from 0.1 to 0.3 (Table 5). The correlations among the MODIS, MISR, WRF-Chem, and observed AODs are all not significant. However, the variation in the modeled AOD is closer to that of the MODIS AOD. The AOD at Nam Co is the lowest with an average of 0.05 due to lower local emissions (Table 5). Both MODIS and MISR AOD show large divergences and the correlation coefficients are not significant at Nam Co. In contrast, AOD from the WRF-Chem model is the closest to the observation with a correlation coefficient of 0.58 (Table 4).

The wind speed and temperature at 500 hPa were also compared by Chen et al. (2017a,c), and they are consistent with the NCEP FNL data over the East Asia.

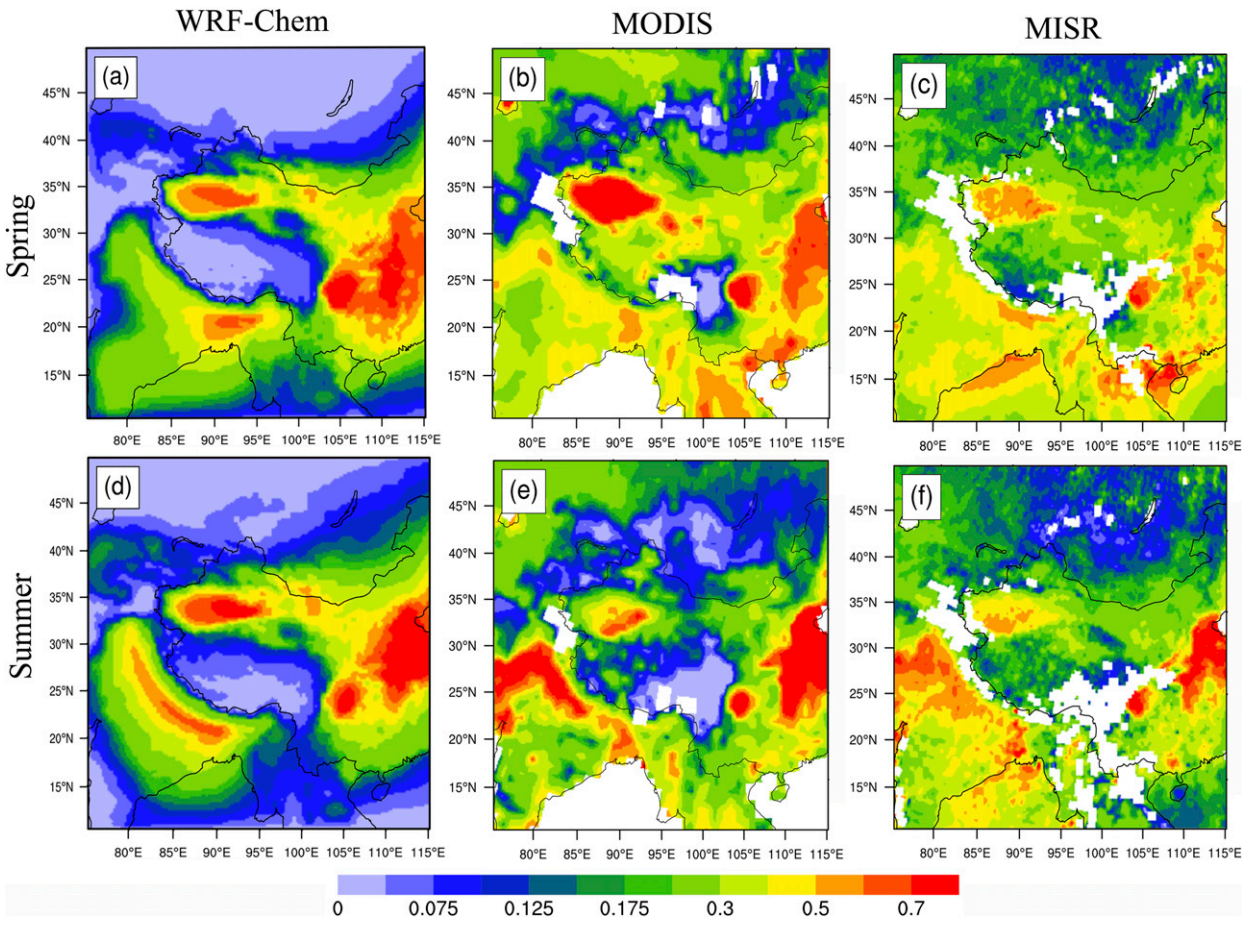

FIG. 4. Spatial distributions of the aerosol optical depth (AOD) at 550 nm from (a),(d) WRF-Chem simulations, (b),(e) MODIS on board *Aqua*, and (c),(f) MISR in the (top) spring and (bottom) summer during the simulation periods.

Overall, the WRF-Chem model is capable of reproducing the three-dimensional structure and temporal variations of meteorological and aerosol fields within the modeling domain. The better performance of the WRF-Chem model will provide more confidence for further investigation of TD dust emission and transport.

b. Emission and transport of TD dust

The spring dust storm events over East Asia occur most frequently from early April to early May (Zhao et al. 2006; Huang et al. 2014). More than 20 severe dust storms occur over the TD and GD annually (Qian et al. 2006), from which approximately 70.54 Tg yr^{-1} of dust is emitted from the TD in the spring, accounting for 42% of the total emitted dust over East Asia (Chen et al. 2017a). The surface easterly wind is dominant in the spring and summer over the TD (Figs. 7a,b), which is consistent with the results of Chen et al. (2017b) and Ge et al. (2014). Influenced by the surface easterly wind, the dust emission fluxes over the TD are 7.8 and 6.3 $\mu g\,m^{-2}\,s^{-1}$ in the spring and summer, respectively. The maximum dust emission can reach up to 73.6 $\mu g\,m^{-2}\,s^{-1}$ in the TD, followed by the GD (54.0 $\mu g\,m^{-2}\,s^{-1}$) in the spring (Figs. 7a,b), and it decreases to 62.2 and 32.5 $\mu g\,m^{-2}\,s^{-1}$ in the TD and GD in the summer, respectively, due to the low frequency of cold fronts (Ge et al. 2014). The dust emission flux over the TP occurs mainly in the western and northern parts of the plateau, and it can reach up to 2 $\mu g\,m^{-2}\,s^{-1}$ in the spring under the strong westerly wind. However, the emission flux in the summer is less than 1.0 $\mu g\,m^{-2}\,s^{-1}$ in most areas and is accompanied by a weakened surface speed, which may be induced by snowmelt due to the increase of soil moisture and restoration of vegetation over the TP after April (Zhou et al. 2009).

The spatial pattern of dust loading is similar to that of dust emission flux with high-value centers located in the TD and GD (Figs. 7c,d). However, the dust loading over the regions near central Asia (region 1), the TD (region 2), and Mongolia (region 3) in the summer are much larger than those in the spring, where the differences can

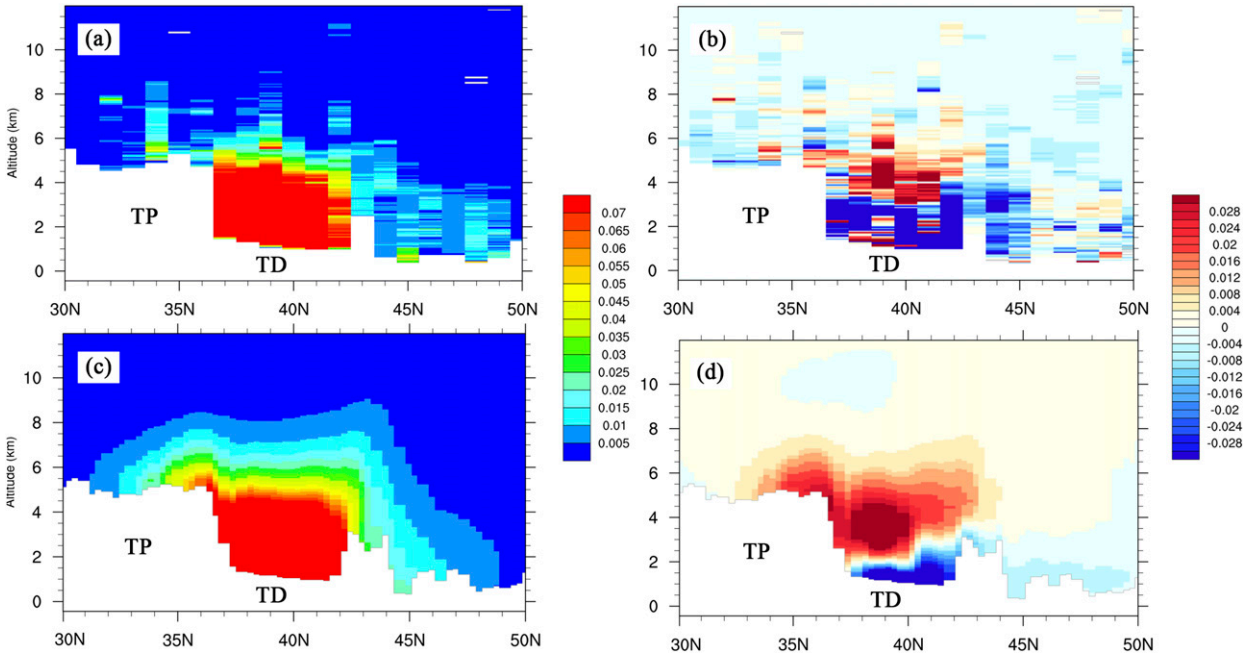

FIG. 5. Cross sections of dust extinction coefficient (km^{-1}) at 532 nm for (a),(c) summer and (b),(d) differences (summer minus spring) along 84°E from (top) *CALIPSO* and (bottom) the WRF-Chem model during the simulation periods, respectively. White color indicates the topography.

reach up to 90 mg m^{-2} (Fig. 7e). In region 1, most of the dust storms occur from April to September, and the largest deposition mainly appears during the summer (Indoitu et al. 2012; Groll et al. 2013; Rashki et al. 2018), where the dust emission flux in the spring is slightly lower than that in the summer (Figs. 7a,b), leading to higher dust loading in that season. In regions 2 and 3, the magnitudes of dust emissions in the summer are smaller than those in the spring. However, TD dust particles are not easily transported to remote regions; rather, they are accumulated in the atmosphere near source regions due to the weakness of the westerly wind in the summer and the complexity of the terrain (Chen et al. 2017a). Simultaneously, because of the different circulation patterns in the two seasons, the dust from the TD and GD can be transported northeastward to Mongolia, resulting in higher dust loading in region 3 (Chen et al. 2018).

To investigate the seasonal differences in the dust loading over the TD in more detail, the vertical profile of the TD dust transport flux above 3 km and the net dust

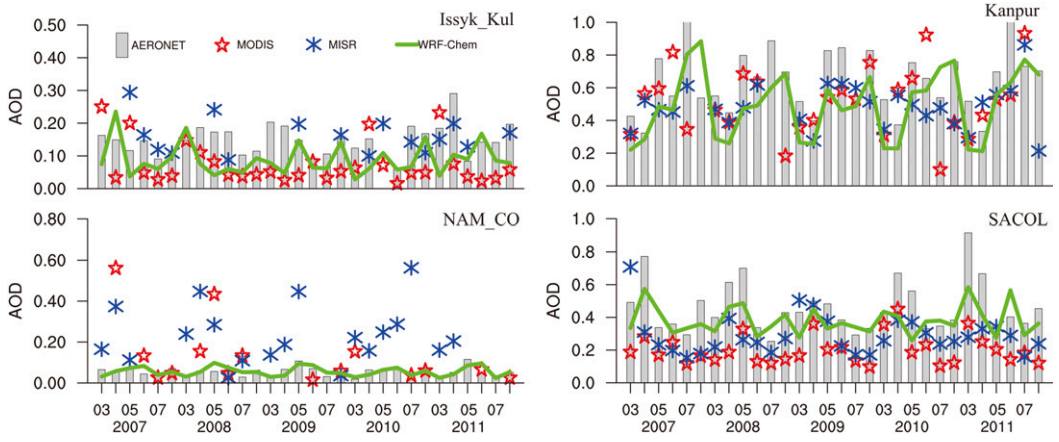

FIG. 6. Monthly variations of AOD at 550 nm from AERONET observations at four sites (Issyk-Kul, Kanpur, Nam Co, and SACOL), MODIS on board *Aqua*, MISR, and the WRF-Chem model during the simulation periods.

TABLE 4. The correlation coefficients of the AODs between four AERONET sites and the WRF-Chem model, MISR, and MODIS results. An asterisk (*) indicates that the correlation passes the 95% significance level.

	WRF-Chem	MISR	MODIS
SACOL	0.63*	0.34	0.67*
Kanpur	0.65*	0.39	0.24
Nam Co	0.58*	0.60	−0.19
Issyk-Kul	0.10	0.16	0.20

transport flux in the four edges of the TD in both the spring and the summer based on the WRF-Chem model are shown in Fig. 8 and Table 6, respectively. The characteristics of TD dust transport in the different directions are as follows. 1) Eastward transport: The magnitude of the dust transport flux in the spring is much larger than that in the summer at 3–6.5 km with net fluxes of 1.67 and 1.11 $g\,m^{-1}\,s^{-1}$ in the spring and summer (Table 6), respectively. However, the altitude of the peak dust transport flux in the summer increases to 5 km, which is higher than that in the spring (Fig. 8a). 2) Southward transport: Although the southward transport of TD dust exhibits a smaller intensity than the eastward transport in the spring, the maximum dust transport flux in the summer increases to 340 $\mu g\,m^{-2}\,s^{-1}$, which is comparable to that of the eastward transport at certain altitude in the summer. The net dust transport fluxes in the spring and summer are 0.46 and 0.53 $g\,m^{-1}\,s^{-1}$, respectively (Table 6). In addition, the higher dust transport flux in the summer mainly appears at 3–4.5 km (Fig. 8b). 3) Northward transport: The northward transport of TD dust in the summer also increases at 3.5–6 km, and the net dust fluxes in the spring and summer are 0.11 and 0.16 $g\,m^{-1}\,s^{-1}$, respectively (Table 6), which are lower than those in the first two directions (Fig. 8c). 4) Westward transport: The net dust transport fluxes in the spring and summer are opposite to those in the other three directions and are the smallest among the four directions (Table 6), indicating that the westward transport of TD dust has only a slight effect on the overall transport of TD dust (Fig. 8d).

Overall, except for the eastward transport, which has been investigated by numerous studies, the meridional transport of dust particles originating from the TD cannot be ignored, especially during the summertime. The total dust transport fluxes outside of the TD are 2.24 and 1.79 $g\,m^{-1}\,s^{-1}$ in the spring and summer, respectively (Table 6). Almost 74% (61%) of the dust is transported eastward, 21% (30%) is transported southward, and 5% (9%) is transported northward in spring (summer). Interestingly, the meridional transport of TD dust is the second highest, especially for southward transport, whereas the intensities of northward and westward transport are relatively small, indicating that the southward transport of TD dust can contribute substantial dust to the TP in the summer.

c. *The mechanism of TD dust transport*

To further investigate the TD dust transport mechanism, the associated thermal and dynamic factors are investigated in this section. The vertical cross section of the dust concentration, the meridional circulation, and the zonal wind along 84°E are shown in Fig. 9. It is obvious that the location and intensity of the westerly jet in summer are different from that in spring. Zhang et al. (2008) argued that the core of the East Asian westerly jet at 200 hPa occurred over Japan in winter and over northwest China in summer. The intensity of westerly jet at 200 hPa along 90°E weakened from January to May and began to increase slowly on July. The peak wind speed in spring and summer ranged from 25 to 35 $m\,s^{-1}$, which is consistent with our results (Fig. 9). The westerly jet along 84°E is located at 31°N in spring and it shifts north to 40°N in summer. The wind speed in summer at 3–8 km is 0–4 $m\,s^{-1}$ lower than that in spring, indicating the westerly wind weakens (Fig. 9c). The peak dust concentration, which is more than 245 $\mu g\,m^{-3}$, is mainly located below 3 km in spring due to the strong westerly wind at 5 km (5–10 $m\,s^{-1}$). In contrast, it extends up to 4 km in summer along with the weakness of westerly wind. Moreover, the dust concentration over northern TP and Tianshan Mountains reaches up to 85 $\mu g\,m^{-3}$ in summer whereas it is only up to 45 $\mu g\,m^{-3}$ in spring. The difference of dust concentration shows large positive values appearing above 3 km, of more than 30 $\mu g\,m^{-3}$, indicating that the dust can be easily lifted to middle

TABLE 5. The AOD statistics from the AERONET sites, WRF-Chem simulations, and MODIS and MISR retrievals.

	AERONET		WRF-Chem		MISR		MODIS	
Sites	Average	Std dev	Average	Std dev	Average	Std dev	Average	Std dev
SACOL	0.46	0.16	0.38	0.09	0.29	0.12	0.21	0.09
Kanpur	0.65	0.20	0.50	0.21	0.48	0.14	0.52	0.21
Nam Co	0.05	0.02	0.06	0.02	0.27	0.23	0.19	0.27
Issyk-Kul	0.15	0.05	0.09	0.05	0.16	0.06	0.08	0.06

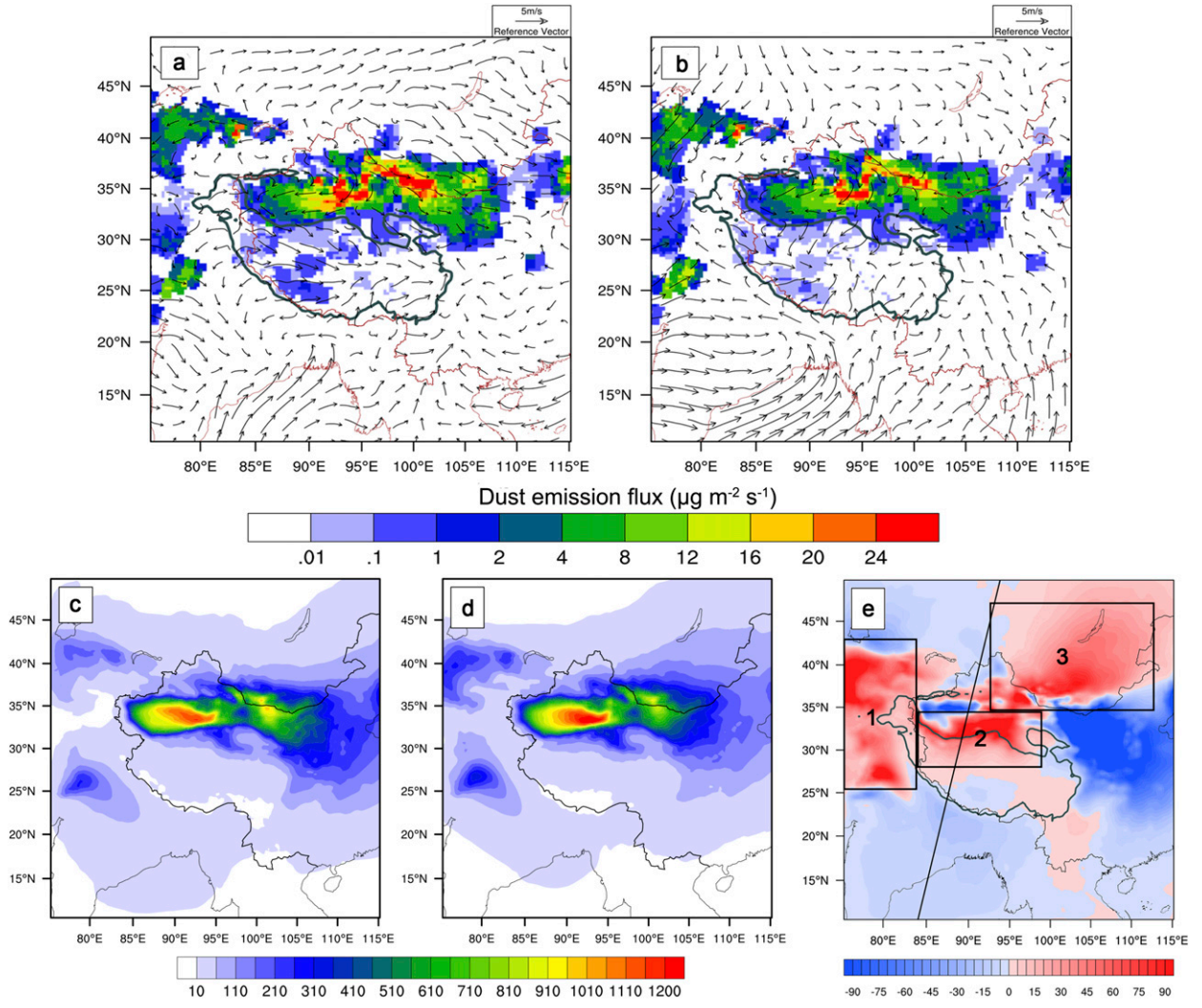

FIG. 7. Spatial distribution of dust emissions (units: $\mu g\,m^{-2}\,s^{-1}$) and wind vectors at 10 m in the (a) spring and (b) summer and the dust mass loading (units: $mg\,m^{-2}$) in (c) spring and (d) summer, as well as the (e) seasonal difference (summer minus spring) in the modeling domain during the simulation periods [the black line in (e) is the cross section of 84°E].

troposphere and accumulates over the TD and its surrounding areas in summer. This difference is also demonstrated from the *CALIPSO* observations (Fig. 5b). The strong negative difference of dust concentration below 3 km can be attributed to the large dust emission in spring. Therefore, the north shift and weakness of westerly jet are responsible for the large concentration of the dust layer over the TD and the decrease of eastward transport of TD dust in summer.

The large positive dust layer can also extend to the northern TP and Tianshan Mountains, indicating that meridional transport is remarkable in summertime. It is worth noting that the strong south wind anomaly is dominant from the TD to the Tianshan Mountains, which is beneficial for the northward transport, leading to the higher dust concentration in summer (Fig. 9c). Numerical studies and satellite retrievals have indicated that dust particles over the TP are primarily contributed from local emissions in the spring, whereas they are mainly contributed from nearby dust sources in the summer, among which the TD is a major contributor (Chen et al. 2014b; Mao et al. 2013; Huang et al. 2007; Kang et al. 2016). The southward transport of TD dust in summer is highly related to the circulation pattern change over the TP. The strong ascent motion is located over the TP and it expands from near the surface to the top of troposphere during summertime (Fig. 9b). Moreover, both easterlies and westerlies are notable at the top of troposphere, resulting from the South Asian high.

To reveal the circulation pattern of the TD dust transport, the wind field and dust concentration at 500 hPa are shown in Fig. 10. Large dust concentrations also exist over

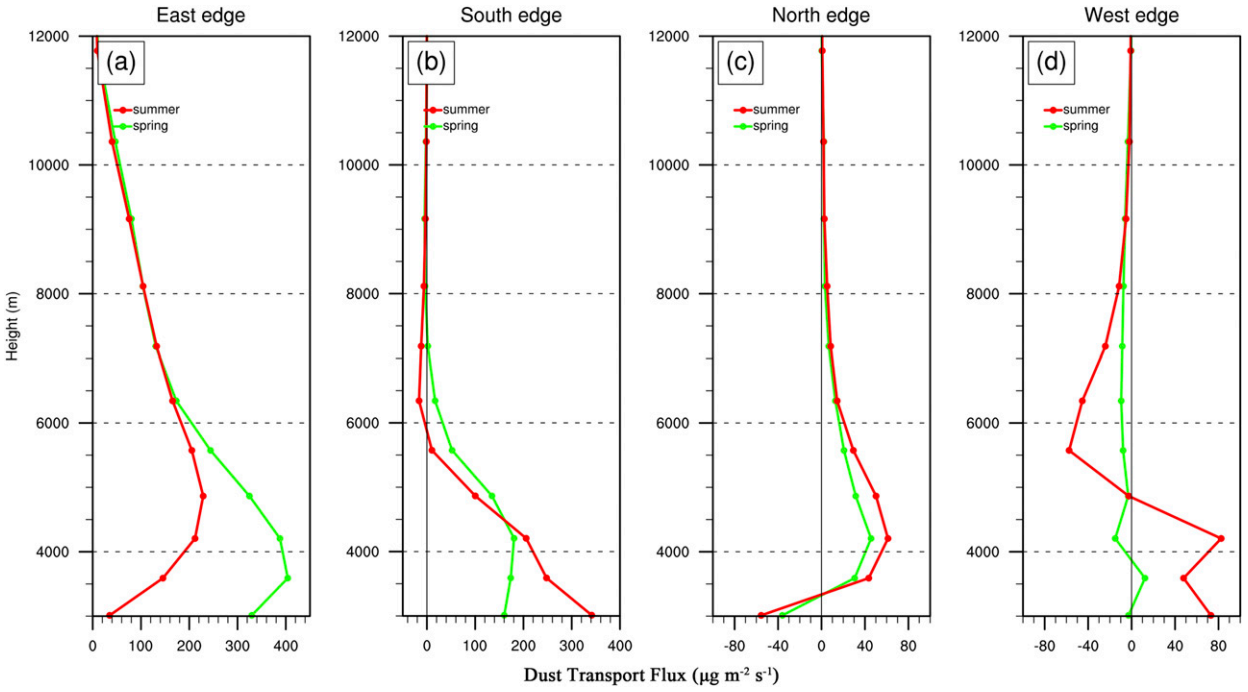

FIG. 8. Vertical distribution of TD dust transport flux ($\mu g\,m^{-2}\,s^{-1}$) in the four edges in Fig. 1 of the TD in the spring (red) and summer (green) above 3 km during the simulation periods. Positive (negative) transport flux indicates the dust is transported out of (into) the TD. On the east edge, positive transport flux indicates the dust is transported eastward to eastern China; on the south edge, positive transport flux indicates the dust is transported southward to the northern TP; on the north edge, positive transport flux indicates the dust is transported northward to the Tianshan Mountains; and on the west edge, positive transport flux indicates the dust is transported westward to Pamir.

the TD and northern TP at 500 hPa in summer, which is higher than that in spring when the dust concentration is 20–25 $\mu g\,m^{-3}$ over the TD and 35–40 $\mu g\,m^{-3}$ over the northern TP. Cyclonic convergence appears over the TP in the summer (Fig. 10b), especially near the surface (Fig. 7b), causing a weak northerly wind over the northern TP. The dust particles accumulating in the atmosphere over the TD can then be transported southward to the northern TP by this northerly wind and topographic uplift, leading to higher dust concentrations exceeding 50 $\mu g\,m^{-3}$ (Fig. 9b). Simultaneously, the strong anticyclone (South Asian high) at the top of troposphere is beneficial for maintaining the surface convergence, which may result in more dust input to the TP. In contrast, only a small portion of dust can be transported to the northern TP where the dust concentration is only below 40 $\mu g\,m^{-3}$ due to the strong westerly winds at the middle to upper troposphere during the spring (Figs. 9a and 10a). In addition, the dust concentration extends northeast from the TD to Mongolia at 500 hPa in summer, whereas it extends to northern China in spring. Therefore, the differences of dust mass loading are positive in Mongolia and negative in northern China (Fig. 7e).

TABLE 6. The vertical integration of the dust flux (units: $g\,m^{-1}\,s^{-1}$) above 3 km in the different edges of the TD [the blue box shown in Fig. 1; positive (negative) values indicate the dust is transported out of (into) the TD].

Flux ($g\,m^{-1}\,s^{-1}$)	East	South	West	North	Total
Spring	1.67	0.46	−0.05	0.11	2.19
Summer	1.11	0.53	0	0.16	1.80

The special circulation pattern over the TP is associated with the surface sensible heating and latent heating and they play important roles in TD dust transport. The sensible heat flux increases substantially from March to July with a maximum flux of 75.46 $W\,m^{-2}$ on July over the TD, which leads to an increase of the planetary boundary layer height (PBLH) to 921 m. The latent heat flux is much lower than the sensible flux due to the low precipitation over arid regions (Fig. 11a). Under these circumstances dust particles can be easily entrained to 5 km under the strong turbulent mixing and vertical motion in the summer, resulting in high dust concentration at 3–8 km (Fig. 9c). Both sensible and latent heat fluxes over the northern TP increase from March to July, and a larger flux is registered from May to August. However, the sensible heating is much larger than the latent heating

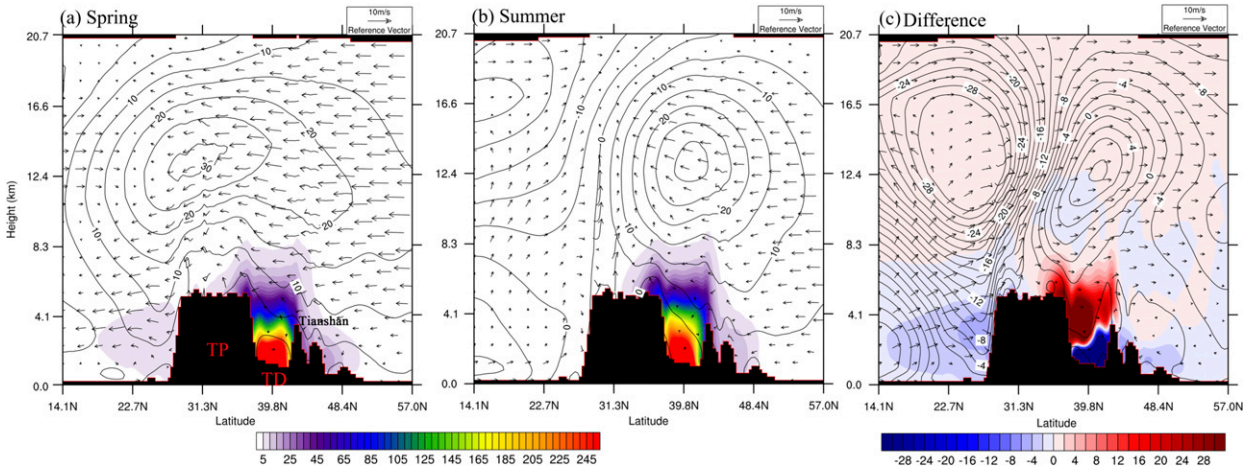

FIG. 9. Cross sections of dust concentration (colors; $\mu g\,m^{-3}$), meridional circulation (vectors), and zonal wind (contour lines; $m\,s^{-1}$) in (a) the spring and (b) summer, and (c) the difference (summer minus spring) along 84°E during the simulation periods from the WRF-Chem model.

with maximum fluxes of 85.18 and 32.97 $W\,m^{-2}$ respectively in July over the northern TP (Fig. 11b). Wu et al. (2016) noted that the summertime sensible heating can significantly intensify the vertical motion and near-surface convergence over the TP compared with the latent heating. Therefore, the intense updraft and surface convergence are formed by strong sensible heating in summer. Simultaneously, the PBLH increases significantly from May to August and the dust mass loading maintains large values of 92–97 $mg\,m^{-2}$ between May and August (Fig. 11b). The dust can then is transported to the altitude of 8 km by the turbulent mixing in PBL and strong vertical motion (Chen et al. 2013).

d. *Observation evidence for the summer TD dust meridional transport*

Since local dust emission is much lower and the dust over the TP originating from the TD is large in summer, two high (2008 and 2009) and two low (2007 and 2012) dust summers with dust AOD anomalies over the northern TP

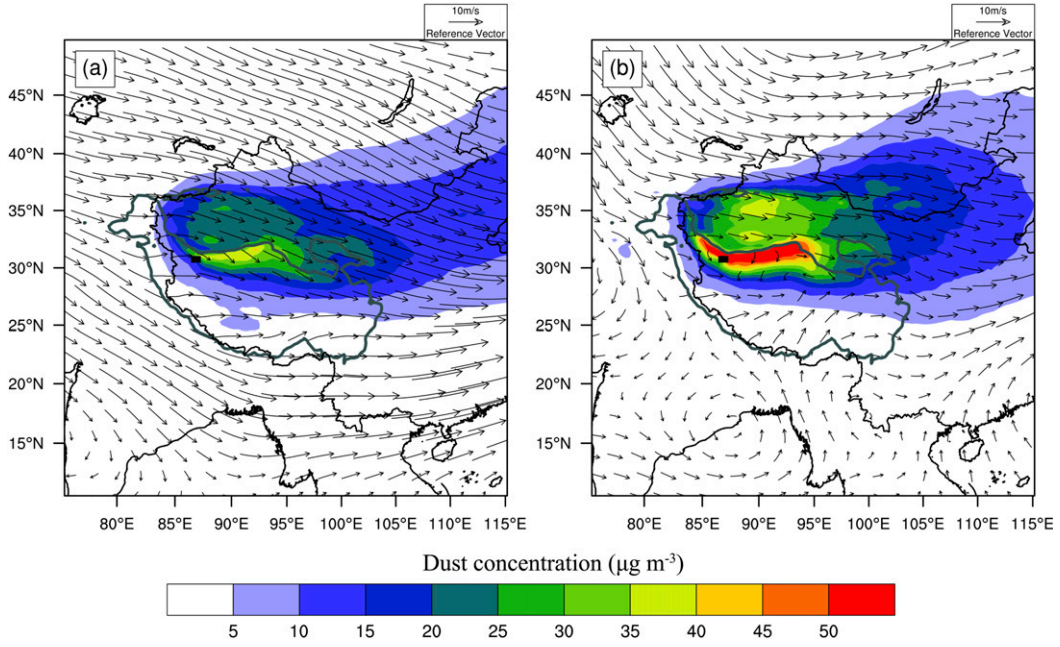

FIG. 10. Spatial distributions of horizontal wind vectors and dust concentration ($\mu g\,m^{-3}$) at 500 hPa in (a) spring and (b) summer during the simulation periods from the WRF-Chem model.

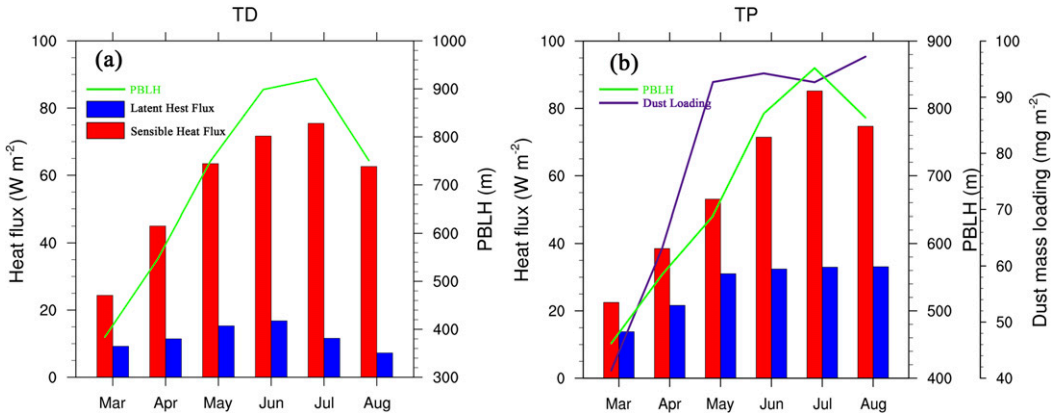

FIG. 11. Monthly variations of sensible heat and latent heat flux ($W\,m^{-2}$), PBLH (m), and dust mass loading ($mg\,m^{-2}$) over the (a) TD and (b) northern TP. The locations of the TD and northern TP are shown in Fig. 1.

larger than one standard deviation are selected for composite purposes to reveal the relationship of the summer TP dust with sensible heating and atmospheric circulation based on 10-yr dust AOD detected from *CALIPSO* from 2007 to 2016. Figure 12 presents the cross section of DEC over the TP averaged from 80° to 95°E in high and low dust summers. Positive anomalies are found over the northern TP and the south of the TD, especially at the altitudes of 2–9 km where the anomalies of DEC can reach up to $0.01\,km^{-1}$, indicating that the magnitudes of the dust from the TD increase over the TP and the south of TD in high dust summers. On the contrary, negative anomalies cover the whole northern TP and the south of TD in low dust summers, which indicates that dust storms are rare.

In high dust summers, a strong negative geopotential height anomaly center appears at the northeast of Kazakhstan (55°–60°N, 80°–90°E), where the negative anomaly temperature is more than 1.0°C, which indicates the cold air is strong here. The intensified cold air can expand southward to the TD (Figs. 13a,c) and benefit the outbreak of the dust storms, leading to higher DEC (Fig. 12a). The weak positive geopotential height anomaly as well as the increase of temperature over the Pamir strengthen the northeast wind at 500 hPa. Thus, the westerly wind weakens and the north wind increases. Moreover, a cyclonic circulation anomaly appeared at the western TP, which favors the southward transport of TD dust (Fig. 13e). Correspondingly, the sensible heat flux increases by 3–9 $W\,m^{-2}$ over the TD and north slopes of the TP, which can enhance the air ascending through the TP sensible heat driving air pump (Wu et al. 2007). Most dust particles will be lifted into atmosphere over the TD and transported southward to the northern TP through strong sensible heating and northeast wind. In low dust summers, a positive geopotential height anomaly center also occurs at the north of Kazakhstan, and the positive temperature anomaly is high. Thus, the cold air is weakened and the DEC is low over the TD and northern TP (Fig. 12b). Moreover, both the north wind and the sensible heat flux also are weaker than

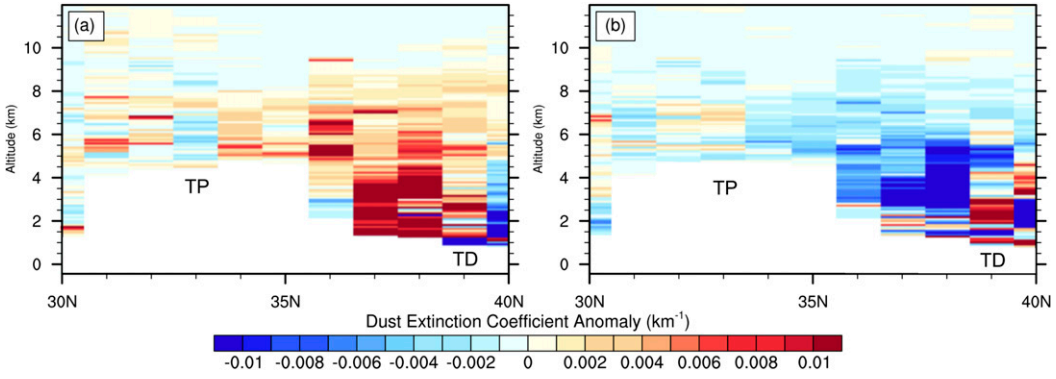

FIG. 12. Composites of summertime dust extinction coefficient (km^{-1}) at 532 nm anomalies averaged from 80° to 95°E detected from *CALIPSO* in (a) high dust summers and (b) low dust summers over northern TP during 2007–16. White color indicates the topography.

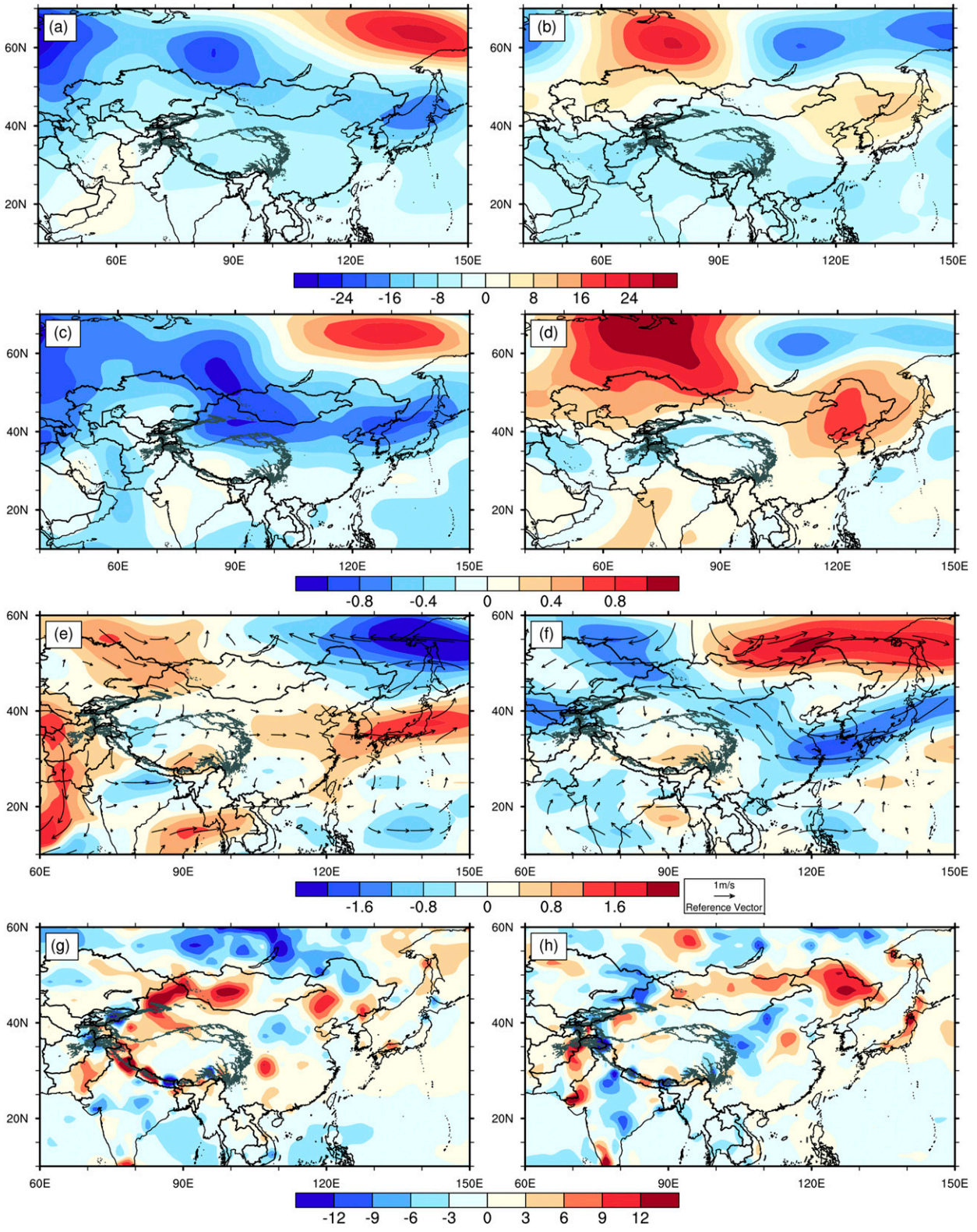

FIG. 13. Composites of summertime anomalies for (a),(b) geopotential height (gpm), (c),(d) air temperature (°C), (e),(f) wind field ($m\,s^{-1}$) at 500 hPa, and (g),(h) surface sensible heat flux ($W\,m^{-2}$) in (left) high dust summers and (right) low dust summers over northern TP during 2007–16.

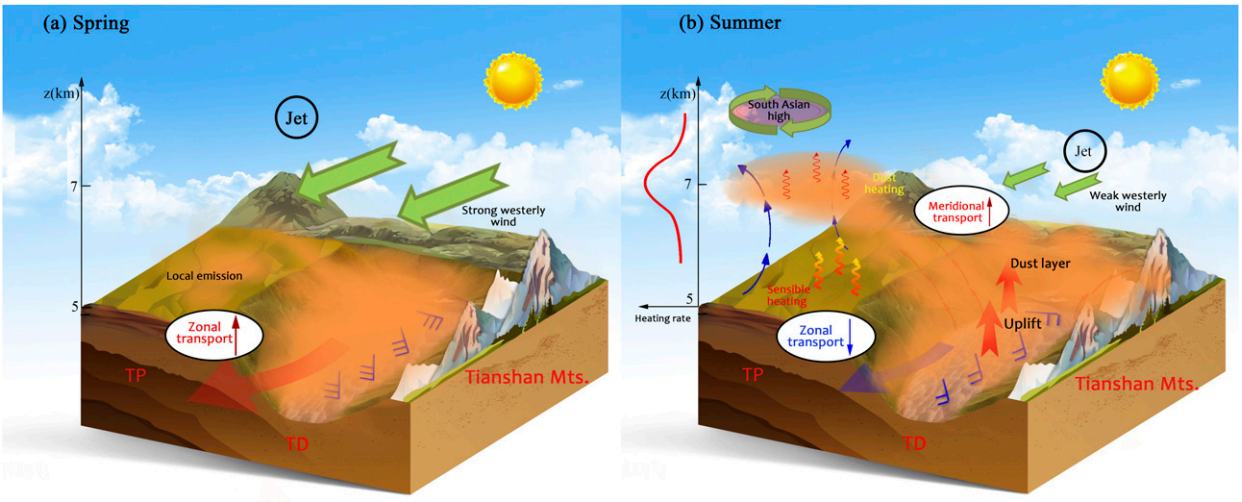

FIG. 14. Schematic diagram of TD dust transport in (a) spring and (b) summer.

those in high dust summer, which is unfavorable for the dust emission and southward transport.

4. Conclusions and discussion

The WRF-Chem model was used to investigate the characteristics of the transport of TD dust in the four cardinal edges of the TD, especially for the meridional transport during the spring and summer in this study. Through comparisons with satellite retrievals, in situ observations, and reanalysis data, the results show that the WRF-Chem model has the ability to reproduce the spatial and temporal distributions of aerosols and meteorological fields in the modeling domain during 2007–11, which is beneficial for understanding the transport of TD dust. Dust emission flux over the TD and TP in summer is lower than that in spring. In contrast, the dust mass loading in summer is 90 mg^{-2} higher than that in spring over the northern TP, Tianshan Mountains, and Mongolia. Satellite observations also confirm that dust over the TD can extend to the TP and Tianshan Mountains. Through the analysis of TD dust transport in the four edges we found that although the magnitudes of eastward transport of TD dust are the largest in both seasons, the meridional transport of TD dust cannot be ignored, especially during the summertime. The magnitudes of the eastward transport of TD dust account for 74% (61%) in spring (summer), while the southward and northward transports of TD dust account for 21% (30%), and 5% (9%), respectively. Notably, the meridional transport of TD dust is the second largest, especially in the summer, when there is a decrease in the eastward transport of TD dust.

The seasonal differences of the meridional transport of TD dust are associated with the seasonal circulation change and thermal forcing (Fig. 14). During the springtime (Fig. 14a), dust particles do not easily accumulate over the TD due to the strong westerly wind and small sensible heating, although the dust emission is strong. A large portion of dust from the TD is transported eastward to eastern China. Only a small portion of dust is transported to the northern TP and Tianshan Mountains by topographic uplift and weak sensible heating. At this time, the TP is a dust source and most of the dust is transported to the Pacific Ocean by the strong westerly wind (Fang et al. 2004). On the contrary, TD dust is easily lifted to 5 km under the strong sensible heating in summer (Fig. 14b). The magnitude of eastward transport of TD dust decreases by about 34% and most dust is accumulated at 3–8 km owing to the north shift and weakness of westerly wind, which provide the foundation for meridional transport. By the south wind anomaly, dust transported to Tianshan Mountains increases in summer. The enhancement of the sensible heating flux in the summer can lead to a convergence field near the surface. Therefore, the cyclonic convergence at the surface and anticyclone divergence at the top of troposphere over the TP are beneficial for southward transport and uplift. The dust particles can be lifted up to 8 km, upon which they can heat the atmosphere by absorbing solar radiation, further enhancing the heating source of the TP.

Composite analysis for high and low dust summers over the northern TP from 2007 to 2016 also confirms the model results. In summer, the enhanced cold air over the northeast of Kazakhstan causes the increase of dust storms and north wind. Simultaneously, the strong sensible heating

over the TD can entrain more dust particles into high altitudes, which is favorable for the dust emission and southward transport of dust over the TD. It should be noted that the sensible heating on the sloping surfaces of the TP has significant effects on the atmosphere circulation over Asia. Under the sensible heating on the sloping surface of TP, the air in the lower atmosphere in the surrounding areas of TP can be driven into the TP, forming strong ascending air (Wu et al. 2007), which will carry more dust to TP. The increase of dust over the TP may further enhance the "elevated heat pump" (Lau et al. 2006, 2008) and have a positive feedback to the southward transport of TD dust. In addition, the dust deposited on snow/ice over the TP can also change the surface albedo, leading to a positive temperature anomaly (Ji et al. 2016), which may further modify the hydrologic cycle and the Asian monsoon climate (Lau et al. 2010; Qian et al. 2011; Sun and Liu 2016; Han et al. 2009; Li et al. 2017).

Acknowledgments. This research was supported by the Foundation for National Natural Science Foundation of China (41775003), Innovative Research Groups of the National Science Foundation of China (Grant 41521004), and the China 111 Project (B13045) and Foundation of Key Laboratory for Semi-Arid Climate Change of the Ministry of Education in Lanzhou University (lzujbky-2017-kb02).

REFERENCES

Bi, J., J. Huang, Q. Fu, X. Wang, J. Shi, W. Zhang, Z. Huang, and B. Zhang, 2011: Toward characterization of the aerosol optical properties over Loess Plateau of northwestern China. *J. Quant. Spectrosc. Radiat. Transfer*, **112**, 346–360, https://doi.org/10.1016/j.jqsrt.2010.09.006.

Chen, F., and J. Dudhia, 2001: Coupling an advanced land surface–hydrology model with the Penn State–NCAR MM5 modeling system. Part I: Model implementation and sensitivity. *Mon. Wea. Rev.*, **129**, 569–585, https://doi.org/10.1175/1520-0493(2001)129<0569:CAALSH>2.0.CO;2.

——, and Coauthors, 1996: Modeling of land surface evaporation by four schemes and comparison with FIFE observations. *J. Geophys. Res.*, **101**, 7251–7268, https://doi.org/10.1029/95JD02165.

Chen, S., J. Huang, C. Zhao, Y. Qian, L. R. Leung, and B. Yang, 2013: Modeling the transport and radiative forcing of Taklimakan dust over the Tibetan Plateau: A case study in the summer of 2006. *J. Geophys. Res. Atmos.*, **118**, 797–812, https://doi.org/10.1002/jgrd.50122.

——, and Coauthors, 2014a: Regional modeling of dust mass balance and radiative forcing over East Asia using WRF-Chem. *Aeolian Res.*, **15**, 15–30, https://doi.org/10.1016/j.aeolia.2014.02.001.

——, J. Huang, Y. Qian, J. Ge, and J. Su, 2014b: Effects of aerosols on autumn precipitation over mid-eastern China. *J. Trop. Meteor.*, **20**, 242–250.

——, ——, J. Li, R. Jia, N. Jiang, L. Kang, X. Ma, and T. Xie, 2017a: Comparison of dust emission, transport, and deposition between the Taklimakan Desert and Gobi Desert from 2007 to 2011. *Sci. China Earth Sci.*, **60**, 1338–1355, https://doi.org/10.1007/s11430-016-9051-0.

——, and Coauthors, 2017b: An overview of mineral dust modeling over East Asia. *J. Meteor. Res.*, **31**, 633–653, https://doi.org/10.1007/s13351-017-6142-2.

——, and Coauthors, 2017c: Emission, transport, and radiative effects of mineral dust from the Taklimakan and Gobi Deserts: Comparison of measurements and model results. *Atmos. Chem. Phys.*, **17**, 2401–2421, https://doi.org/10.5194/acp-17-2401-2017.

——, and Coauthors, 2018: Dust modeling over East Asia during the summer of 2010 using the WRF-Chem model. *J. Quant. Spectrosc. Radiat. Transfer*, **213**, 1–12, https://doi.org/10.1016/j.jqsrt.2018.04.013.

Cheng, T., H. Chen, X. Gu, T. Yu, J. Guo, and H. Guo, 2012: The intercomparison of MODIS, MISR and GOCART aerosol products against AERONET data over China. *J. Quant. Spectrosc. Radiat. Transfer*, **113**, 2135–2145, https://doi.org/10.1016/j.jqsrt.2012.06.016.

Diner, D., J. Martonchik, R. Kahn, B. Pinty, N. Gobron, D. Nelson, and B. Holben, 2005: Using angular and spectral shape similarity constraints to improve MISR aerosol and surface retrievals over land. *Remote Sens. Environ.*, **94**, 155–171, https://doi.org/10.1016/j.rse.2004.09.009.

Dubovik, O., and M. King, 2000: A flexible inversion algorithm for retrieval of aerosol optical properties from sun and sky radiance measurements. *J. Geophys. Res.*, **105**, 20 673–20 696, https://doi.org/10.1029/2000JD900282.

Duce, R., C. Unni, B. Ray, J. Prospero, and J. Merrill, 1980: Long-range atmospheric transport of soil dust from Asia to the tropical North Pacific: Temporal variability. *Science*, **209**, 1522–1524, https://doi.org/10.1126/science.209.4464.1522.

Fang, X., Y. Han, J. Ma, L. Song, S. Yang, and X. Zhang, 2004: Dust storms and loess accumulation on the Tibetan Plateau: A case study of dust event on 4 March 2003 in Lhasa. *Chin. Sci. Bull.*, **49**, 953–960, https://doi.org/10.1007/BF03184018.

Fast, J., J. Gustafson, R. Easter, R. Zaveri, J. Barnard, E. Chapman, G. Grell, and S. Peckham, 2006: Evolution of ozone, particulates, and aerosol direct radiative forcing in the vicinity of Houston using a fully coupled meteorology–chemistry–aerosol model. *J. Geophys. Res.*, **111**, D21305, https://doi.org/10.1029/2005JD006721.

Fu, Q., and Coauthors, 2010: Source, long-range transport, and characteristics of a heavy dust pollution event in Shanghai. *J. Geophys. Res.*, **115**, D00K29, https://doi.org/10.1029/2009JD013208.

Gao, Y., M. Zhang, X. Liu, and L. Wang, 2016: Change in diurnal variations of meteorological variables induced by anthropogenic aerosols over the North China Plain in summer 2008. *Theor. Appl. Climatol.*, **124**, 103–118, https://doi.org/10.1007/s00704-015-1403-4.

Ge, J., J. Huang, C. Xu, Y. Qi, and H. Liu, 2014: Characteristics of Taklimakan dust emission and distribution: A satellite and reanalysis field perspective. *J. Geophys. Res. Atmos.*, **119**, 11 772–11 783, https://doi.org/10.1002/2014JD022280.

Ginoux, P., M. Chin, I. Tegen, J. Prospero, B. Holben, O. Dubovik, and S. Lin, 2001: Sources and distributions of dust aerosols simulated with the GOCART model. *J. Geophys. Res.*, **106**, 20 255–20 273, https://doi.org/10.1029/2000JD000053.

Grell, G., S. Peckham, R. Schmitz, S. McKeen, G. Frost, W. Skamarock, and B. Eder, 2005: Fully coupled "online" chemistry within the WRF model. *Atmos. Environ.*, **39**, 6957–6975, https://doi.org/10.1016/j.atmosenv.2005.04.027.

Groll, M., C. Opp, and I. Aslanov, 2013: Spatial and temporal distribution of the dust deposition in Central Asia—Results from a long term monitoring program. *Aeolian Res.*, **9**, 49–62, https://doi.org/10.1016/j.aeolia.2012.08.002.

Gu, Y., Y. Xue, F. De Sales, and N. Liou, 2016: A GCM investigation of dust aerosol impact on the regional climate of North Africa and South/East Asia. *Climate Dyn.*, **46**, 2353–2370, https://doi.org/10.1007/s00382-015-2706-y.

Guo, J., and Y. Yin, 2015: Mineral dust impacts on regional precipitation and summer circulation in East Asia using a regional coupled climate system model. *J. Geophys. Res.*, **120**, 10 378–10 398, https://doi.org/10.1002/2015JD023096.

——, K. Rahn, and G. Zhuang, 2004: A mechanism for the increase of pollution elements in dust storms in Beijing. *Atmos. Environ.*, **38**, 855–862, https://doi.org/10.1016/j.atmosenv.2003.10.037.

Han, Y., X. Xi, L. Song, Y. Ye, and Y. Li, 2004: Spatial-temporal sand-dust distribution in Qinhhai-Tibet Plateau and its climatic significance (in Chinese). *J. Desert Res.*, **24**, 588–592.

——, X. Fang, T. Zhao, H. Bai, S. Kang, and L. Song, 2009: Suppression of precipitation by dust particles originated in the Tibetan Plateau. *Atmos. Environ.*, **43**, 568–574, https://doi.org/10.1016/j.atmosenv.2008.10.018.

Holben, B., and Coauthors, 1998: AERONET—A federated instrument network and data archive for aerosol characterization. *Remote Sens. Environ.*, **66**, 1–16, https://doi.org/10.1016/S0034-4257(98)00031-5.

Hong, S., Y. Noh, and J. Dudhia, 2006: A new vertical diffusion package with an explicit treatment of entrainment processes. *Mon. Wea. Rev.*, **134**, 2318–2341, https://doi.org/10.1175/MWR3199.1.

Hsu, N., S. Tsay, M. King, and J. Herman, 2006: Deep Blue retrievals of Asian aerosol properties during ACE-Asia. *IEEE Trans. Geosci. Remote Sens.*, **44**, 3180–3195, https://doi.org/10.1109/TGRS.2006.879540.

——, M. Jeong, C. Bettenhausen, A. Sayer, R. Hansell, C. Seftor, J. Huang, and S. Tsay, 2013: Enhanced Deep Blue aerosol retrieval algorithm: The second generation. *J. Geophys. Res. Atmos.*, **118**, 9296–9315, https://doi.org/10.1002/jgrd.50712.

Huang, J., P. Minnis, B. Lin, T. Wang, Y. Yi, Y. Hu, S. Sun-Mack, and K. Ayers, 2006a: Possible influences of Asian dust aerosols on cloud properties and radiative forcing observed from MODIS and CERES. *Geophys. Res. Lett.*, **33**, L06824, https://doi.org/10.1029/2005GL024724.

——, Y. Wang, T. Wang, and Y. Yi, 2006b: Dusty cloud radiative forcing derived from satellite data for middle latitude region of East Asia. *Prog. Nat. Sci.*, **16**, 1084–1089, https://doi.org/10.1080/10020070612330114.

——, B. Lin, P. Minnis, T. Wang, X. Wang, Y. Hu, Y. Yi, and J. K. Ayers, 2006c: Satellite-based assessment of possible dust aerosols semi-direct effect on cloud water path over East Asia. *Geophys. Res. Lett.*, **33**, L19802, https://doi.org/10.1029/2006GL026561.

——, and Coauthors, 2007: Summer dust aerosols detected from CALIPSO over the Tibetan Plateau. *Geophys. Res. Lett.*, **34**, L18805, https://doi.org/10.1029/2007GL029938.

——, P. Minnis, B. Chen, Z. Huang, Z. Liu, Q. Zhao, Y. Yi, and J. Ayers, 2008a: Long-range transport and vertical structure of Asian dust from CALIPSO and surface measurements during PACDEX. *J. Geophys. Res.*, **113**, D23212, https://doi.org/10.1029/2008JD010620.

——, and Coauthors, 2008b: An overview of the Semi-Arid Climate and Environment Research Observatory over the Loess Plateau. *Adv. Atmos. Sci.*, **25**, 906–921, https://doi.org/10.1007/s00376-008-0906-7.

——, Q. Fu, J. Su, Q. Tang, P. Minnis, Y. Hu, Y. Yi, and Q. Zhao, 2009: Taklimakan dust aerosol radiative heating derived from CALIPSO observations using the Fu–Liou radiation model with CERES constraints. *Atmos. Chem. Phys.*, **9**, 4011–4021, https://doi.org/10.5194/acp-9-4011-2009.

——, P. Minnis, H. Yan, Y. Yi, B. Chen, L. Zhang, and J. Ayers, 2010: Dust aerosol effect on semi-arid climate over northwest China detected from A-Train satellite measurements. *Atmos. Chem. Phys.*, **10**, 6863–6872, https://doi.org/10.5194/acp-10-6863-2010.

——, Q. Fu, W. Zhang, X. Wang, R. Zhang, H. Ye, and S. Warren, 2011: Dust and black carbon in seasonal snow across northern China. *Bull. Amer. Meteor. Soc.*, **92**, 175–181, https://doi.org/10.1175/2010BAMS3064.1.

——, T. Wang, W. Wang, Z. Li, and H. Yan, 2014: Climate effects of dust aerosols over East Asian arid and semiarid regions. *J. Geophys. Res. Atmos.*, **119**, 11 398–11 416, https://doi.org/10.1002/2014JD021796.

——, J. J. Liu, B. Chen, and S. L. Nasiri, 2015: Detection of anthropogenic dust using CALIPSO lidar measurements. *Atmos. Chem. Phys.*, **15**, 11 653–11 665, https://doi.org/10.5194/acp-15-11653-2015.

——, and Coauthors, 2017: Dryland climate change: Recent progress and challenges. *Rev. Geophys.*, **55**, 719–778, https://doi.org/10.1002/2016RG000550.

Iacono, M., E. Mlawer, S. Clough, and J. Morcrette, 2000: Impact of an improved longwave radiation model, RRTM. on the energy budget and thermodynamic properties of the NCAR community climate mode, CCM3. *J. Geophys. Res.*, **105**, 14 873–14 890, https://doi.org/10.1029/2000JD900091.

Indoitu, R., L. Orlovsky, and N. Orlovsky, 2012: Dust storms in Central Asia: Spatial and temporal variations. *J. Arid Environ.*, **85**, 62–70, https://doi.org/10.1016/j.jaridenv.2012.03.018.

Ji, Z., S. Kang, Q. Zhang, Z. Cong, P. Chen, and M. Sillanpää, 2016: Investigation of mineral aerosols radiative effects over High Mountain Asia in 1990–2009 using a regional climate model. *Atmos. Res.*, **178–179**, 484–496, https://doi.org/10.1016/j.atmosres.2016.05.003.

Jia, R., Y. Liu, B. Chen, Z. Zhang, and J. Huang, 2015: Source and transportation of summer dust over the Tibetan Plateau. *Atmos. Environ.*, **123**, 210–219, https://doi.org/10.1016/j.atmosenv.2015.10.038.

Kahn, R. A., B. J. Gaitley, J. V. Martonchik, D. J. Diner, K. A. Crean, and B. Holben, 2005: Multiangle Imaging Spectroradiometer (MISR) global aerosol optical depth validation based on 2 years of coincident Aerosol Robotic Network (AERONET) observations. *J. Geophys. Res.*, **110**, D10S04, https://doi.org/10.1029/2004JD004706.

Kain, J., 2004: The Kain–Fritsch convective parameterization: An update. *J. Appl. Meteor.*, **43**, 170–181, https://doi.org/10.1175/1520-0450(2004)043<0170:TKCPAU>2.0.CO;2.

——, and J. Fritsch, 1990: A one-dimensional entraining/detraining plume model and its application in convective parameterization. *J. Atmos. Sci.*, **47**, 2784–2802, https://doi.org/10.1175/1520-0469(1990)047<2784:AODEPM>2.0.CO;2.

Kalnay, E., and Coauthors, 1996: The NCEP/NCAR 40-Year Reanalysis Project. *Bull. Amer. Meteor. Soc.*, **77**, 437–471, https://doi.org/10.1175/1520-0477(1996)077<0437:TNYRP>2.0.CO;2.

Kameda, T., E. Azumi, A. Fukushima, N. Tang, A. Matsuki, Y. Kamiya, A. Toriba, and K. Hayakawa, 2016: Mineral dust aerosols promote the formation of toxic nitropolycyclic aromatic compounds. *Sci. Rep.*, **6**, 24427, https://doi.org/10.1038/srep24427.

Kang, L., J. Huang, S. Chen, and X. Wang, 2016: Long-term trends of dust events over Tibetan Plateau during 1961-2010. *Atmos. Environ.*, **125**, 188–198, https://doi.org/10.1016/j.atmosenv.2015.10.085.

——, S. Chen, J. Huang, S. Zhao, X. Ma, T. Yuan, X. Zhang, and T. Xie, 2017: The spatial and temporal distributions of absorbing aerosols over East Asia. *Remote Sens.*, **9**, 1050, https://doi.org/10.3390/rs9101050.

Kaufman, Y., O. Boucher, D. Tanré, M. Chin, L. Remer, and T. Takemura, 2005: Aerosol anthropogenic component estimated from satellite data. *Geophys. Res. Lett.*, **32**, L17804, https://doi.org/10.1029/2005GL023125.

Lau, K.-M., M. Kim, and K. Kim, 2006: Asian summer monsoon anomalies induced by aerosol direct forcing: The role of the Tibetan Plateau. *Climate Dyn.*, **26**, 855–864, https://doi.org/10.1007/s00382-006-0114-z.

——, and Coauthors, 2008: The Joint Aerosol–Monsoon Experiment: A new challenge in monsoon climate research. *Bull. Amer. Meteor. Soc.*, **89**, 369–383, https://doi.org/10.1175/BAMS-89-3-369.

——, M. Kim, K. Kim, and W. Lee, 2010: Enhanced surface warming and accelerated snow melt in the Himalayas and Tibetan Plateau induced by absorbing aerosols. *Environ. Res. Lett.*, **5**, 025204, https://doi.org/10.1088/1748-9326/5/2/025204.

Li, J., Z. Wang, G. Zhuang, G. Luo, Y. Sun, and Q. Wang, 2012: Mixing of Asian mineral dust with anthropogenic pollutants over East Asia: A model case study of a super-duststorm in March 2010. *Atmos. Chem. Phys.*, **12**, 7591–7607, https://doi.org/10.5194/acp-12-7591-2012.

——, Q. Lv, M. Zhang, T. Wang, K. Kawamoto, S. Chen, and B. Zhang, 2017: Effects of atmospheric dynamics and aerosols on the fraction of supercooled water clouds. *Atmos. Chem. Phys.*, **17**, 1847–1863, https://doi.org/10.5194/acp-17-1847-2017.

Li, X., X. Xia, S. Wang, J. Mao, and Y. Liu, 2012: Validation of MODIS and deep blue aerosol optical depth retrievals in an arid/semi-arid region of northwest China. *Particuology*, **10**, 132–139, https://doi.org/10.1016/j.partic.2011.08.002.

Liu, X., Q. Chen, H. Che, R. Zhang, K. Gui, H. Zhang, and T. Zhao, 2016: Spatial distribution and temporal variation of aerosol optical depth in the Sichuan basin, China, the recent ten years. *Atmos. Environ.*, **147**, 434–445, https://doi.org/10.1016/j.atmosenv.2016.10.008.

Liu, Z., and Coauthors, 2008: Airborne dust distributions over the Tibetan Plateau and surrounding areas derived from the first year of CALIPSO lidar observations. *Atmos. Chem. Phys.*, **8**, 5045–5060, https://doi.org/10.5194/acp-8-5045-2008.

Lu, Z., Q. Zhang, and D. Streets, 2011: Sulfur dioxide and primary carbonaceous aerosol emissions in China and India, 1996–2010. *Atmos. Chem. Phys.*, **11**, 9839–9864, https://doi.org/10.5194/acp-11-9839-2011.

Mao, R., D. Gong, Y. Shao, G. Wu, and J. Bao, 2013: Numerical analysis for contribution of the Tibetan Plateau to dust aerosols in the atmosphere over the East Asia. *Sci. China Earth Sci.*, **56**, 301–310, https://doi.org/10.1007/s11430-012-4460-x.

Martonchik, J., D. Diner, K. Crean, and M. Bull, 2002: Regional aerosol retrieval results from MISR. *IEEE Trans. Geosci. Remote Sens.*, **40**, 1520–1531, https://doi.org/10.1109/TGRS.2002.801142.

——, ——, R. Kahn, B. Gaitley, and B. Holben, 2004: Comparison of MISR and AERONET aerosol optical depths over desert sites. *Geophys. Res. Lett.*, **31**, L16102, https://doi.org/10.1029/2004GL019807.

Mlawer, E., S. Taubman, P. Brown, M. Iacono, and S. Clough, 1997: Radiative transfer for inhomogeneous atmospheres: RRTM, a validated correlated-k model for the longwave. *J. Geophys. Res.*, **102**, 16 663–16 682, https://doi.org/10.1029/97JD00237.

Morrison, H., J. Curry, and V. Khvorostyanov, 2005: A new double moment microphysics parameterization for application in cloud and climate models. Part I: Description. *J. Atmos. Sci.*, **62**, 1665–1677, https://doi.org/10.1175/JAS3446.1.

Prospero, J., 1999: Long-term measurements of the transport of African mineral dust to the southeastern United States: Implications for regional air quality. *J. Geophys. Res.*, **104**, 15 917–15 928, https://doi.org/10.1029/1999JD900072.

Qian, Y., M. Flanner, L. Leung, and W. Wang, 2011: Sensitivity studies on the impacts of Tibetan Plateau snowpack pollution on the Asian hydrological cycle and monsoon climate. *Atmos. Chem. Phys.*, **11**, 1929–1948, https://doi.org/10.5194/acp-11-1929-2011.

Qian, Z., Y. Cai, J. Liu, C. Liu, L. Liang, and M. Song, 2006: Some advances in dust storm research over China-Mongolia areas (in Chinese). *Chin. J. Geophys.*, **49**, 68–78, https://doi.org/10.1002/cjg2.813.

Ramanathan, V., P. Crutzen, J. Kiehl, and D. Rosenfeld, 2001: Aerosols, climate, and the hydrological cycle. *Science*, **294**, 2119–2124, https://doi.org/10.1126/science.1064034.

Rashki, A., D. Kaskaoutis, and A. Sepehr, 2018: Statistical evaluation of the dust events at selected stations in southwest Asia: From the Caspian Sea to the Arabian Sea. *Catena*, **165**, 590–603, https://doi.org/10.1016/j.catena.2018.03.011.

Sun, H., and X. Liu, 2016: Numerical modeling of topography-modulated dust aerosol distribution and its influence on the onset of East Asian summer monsoon. *Adv. Meteor.*, **2016**, 6951942, https://doi.org/10.1155/2016/6951942.

Sun, J., M. Zhang, and T. Liu, 2001: Spatial and temporal characteristics of dust storms in China and its surrounding regions, 1960–1999: Relations to source area and climate. *J. Geophys. Res.*, **106**, 10 325–10 333, https://doi.org/10.1029/2000JD900665.

van der Werf, G. R., and Coauthors, 2010: Global fire emissions and the contribution of deforestation, savanna, forest, agricultural, and peat fires (1997–2009). *Atmos. Chem. Phys.*, **10**, 11 707–11 735, https://doi.org/10.5194/acp-10-11707-2010.

Vaughan, M., S. Young, D. Winker, K. Powell, A. Omar, Z. Liu, Y. Hu, and C. Hostetler, 2004: Fully automated analysis of space-based lidar data: An overview of the CALIPSO retrieval algorithms and data products. *Proc. SPIE*, **5575**, 16–30, https://doi.org/10.1117/12.572024.

Wang, S., N. Hsu, S. Tsay, N. Lin, A. Sayer, S. J. Huang, and K. M. Lau, 2012: Can Asian dust trigger phytoplankton blooms in the oligotrophic northern South China Sea? *Geophys. Res. Lett.*, **39**, L05811, https://doi.org/10.1029/2011GL050415.

Wang, X., J. Huang, M. Ji, and K. Higuchi, 2008: Variability of East Asia dust events and their long-term trend. *Atmos. Environ.*, **42**, 3156–3165, https://doi.org/10.1016/j.atmosenv.2007.07.046.

Winker, D. M., J. Pelon, and M. P. McCormick, 2003: The CALIPSO mission: Spaceborne lidar for observation of aerosols and clouds. *Proc. SPIE*, **4893**, 1–11, https://doi.org/10.1117/12.466539.

Wu, G., and Coauthors, 2007: The influence of mechanical and thermal forcing by the Tibetan Plateau on Asian climate. *J. Climate*, **8**, 770–789, https://doi.org/10.1175/JHM609.1.

——, H. Zhuo, Z. Wang, and Y. Liu, 2016: Two types of summertime heating over the Asian large-scale orography and excitation of potential-vorticity forcing I. Over Tibetan Plateau. *Sci. China Earth Sci.*, **59**, 1996–2008, https://doi.org/10.1007/s11430-016-5328-2.

Xia, X., P. Wang, Y. Wang, Z. Li, J. Xin, J. Liu, and H. Chen, 2008: Aerosol optical depth over the Tibetan Plateau and its relation to aerosols over the Taklimakan Desert. *Geophys. Res. Lett.*, **35**, L16804, https://doi.org/10.1029/2008GL034981.

Xu, X., J. Wang, D. Henze, W. Qu, and M. Kopacz, 2013: Constraints on aerosol sources using GEOS-Chem adjoint and MODIS radiances, and evaluation with multisensor (OMI, MISR) data. *J. Geophys. Res. Atmos.*, **118**, 6396–6413, https://doi.org/10.1002/jgrd.50515.

Yuan, T., S. Chen, L. Kang, Z. Chen, Y. Luo, and Q. Zou, 2016: Temporal and spatial distribution characteristics and change trends of dust intensity in dust source regions of China during 1961–2010 (in Chinese). *J. Arid Meteor.*, **34**, 927–935.

Yumimoto, K., K. Eguchi, I. Uno, T. Takemura, Z. Liu, A. Shimizu, and N. Sugimoto, 2009: An elevated large-scale dust veil from the Taklimakan Desert: Intercontinental transport and three-dimensional structure as captured by CALIPSO and regional and global models. *Atmos. Chem. Phys.*, **9**, 8545–8558, https://doi.org/10.5194/acp-9-8545-2009.

Zhang, X., R. Arimoto, and Z. An, 1997: Dust emission from Chinese desert sources linked to variations in atmospheric circulation. *J. Geophys. Res.*, **102**, 28 041–28 047, https://doi.org/10.1029/97JD02300.

Zhang, Y., M. Takahashi, and L. Guo, 2008: Analysis of the East Asian subtropical westerly jet simulated by CCSR/NIES/FRCGC coupled climate system model. *J. Meteor. Soc. Japan*, **86**, 257–278, https://doi.org/10.2151/jmsj.86.257.

Zhao, C., X. Liu, L. Leung, B. Johnson, S. McFarlane, W. Gustafson, J. Fast, and R. Easter, 2010: The spatial distribution of mineral dust and its shortwave radiative forcing over North Africa: Modeling sensitivities to dust emissions and aerosol size treatments. *Atmos. Chem. Phys.*, **10**, 8821–8838, https://doi.org/10.5194/acp-10-8821-2010.

——, ——, ——, and S. Hagos, 2011: Radiative impact of mineral dust on monsoon precipitation variability over West Africa. *Atmos. Chem. Phys.*, **11**, 1879–1893, https://doi.org/10.5194/acp-11-1879-2011.

——, Y. Li, F. Zhang, L. Sun, and P. Wang, 2018: Growth rates of fine aerosol particles at a site near Beijing in June 2013. *Adv. Atmos. Sci.*, **35**, 209–217, https://doi.org/10.1007/s00376-017-7069-3.

Zhao, T., S. Gong, X. Zhang, J. Blanchet, I. McKendry, and Z. Zhou, 2006: A simulated climatology of Asian dust aerosol and its trans-Pacific transport. Part I: Mean climate and validation. *J. Climate*, **19**, 88–103, https://doi.org/10.1175/JCLI3605.1.

Zhou, X., P. Zhao, J. Chen, L. Chen, and W. Li, 2009: Impacts of thermodynamic processes over the Tibetan Plateau on the Northern Hemispheric climate. *Sci. China*, **52D**, 1679–1693, https://doi.org/10.1007/s11430-009-0194-9.